Orbital-Free Density Functional Theory Applied to $NaAlH_4$

Terry J. Frankcombe* and Geert-Jan Kroes

Leiden Institute of Chemistry, Gorlaeus Laboratories, Leiden University, P.O. Box 9502, 2300 RA Leiden, The Netherlands

Nicholas I. Choly and Efthimios Kaxiras

Department of Physics and Division of Engineering and Applied Sciences, Harvard University, Cambridge, Massachusetts 02138

Received: January 11, 2005; In Final Form: July 8, 2005

We present the application of orbital-free density functional theory (OF-DFT) to $NaAlH_4$, a potential hydrogen storage material, and related systems. Although the simple Al and NaH structures are reproduced reasonably well by OF-DFT, the approach fails for the more complex $NaAlH_4$ structure. Calculations on AlH_3 show that the failure to describe the Al−H interaction is related to the kinetic energy functionals used rather than the local pseudopotentials which are required within the OF-DFT approach. Thus, systems such as $NaAlH_4$ present a challenge which awaits the development of more reliable orbital-free kinetic energy functionals.

1. Introduction

Efficient storage of hydrogen has become an important area of development, particularly with a view to using hydrogen as an energy storage medium.[1,2] Storing hydrogen in a solid material is one of the currently preferred methods, with significant advantages over storage based on compressed/liquefied hydrogen or hydrogen-containing liquids. To this end, nanostructured carbon is being heavily investigated as an adsorbent,[1,3−8] while complex metal hydride systems are showing increasing promise.[1,3,4,9−13] The challenge with such hydride systems is to achieve a balance between hydrogen storage capacity and the conditions needed to extract and recharge the hydrogen.

A promising class of hydrides for reversible hydrogen storage are alkali-metal aluminum hydrides, or alanates. Interest in these systems was boosted when Bogdanović and Schwickardi showed that reversible hydrogen cycling in $NaAlH_4$ was facilitated by doping with titanium-based catalysts.[14] Various attempts have been made since then to increase the viability of hydrogen cycling, such as alternate catalytic strategies[15−17] and constituent substitution.[18,19] However, little is known about the atomic-scale mechanism of hydrogen desorption and uptake in these materials[20] and how these processes are affected by the presence of catalysts and constituent substitution.

Clearly, computational methods can significantly contribute to optimizing the design of hydrogen storage materials such as alanates, by studying the effects of catalysts and substituents and by exploring the reaction mechanisms involved. A significant obstacle to using appropriate computational methods is the size of the systems that need to be modeled in order to study the kinetics of solid-phase reactions, which often involve phase separation and phase reassembly. The computational effort required for electronic structure calculations tends to scale with at least the third power of the system size. A pertinent example is density functional theory (DFT).[21,22] Although extremely useful in determining the energetics of various solid-phase structures, the $O(N^3)$ scaling of traditional DFT limits the size of the systems that can be practically studied. A DFT-based approach for calculating electronic energies of solid phases and clusters that exhibits linear scaling with system size would render the modeling of large systems much more efficient, making the modeling of larger systems practical and computational exploration of potential material modifications faster.

A candidate for such a computational method is orbital-free DFT, in which the exact orbital-based kinetic energy (KE) functional of traditional DFT is replaced by an approximate KE functional that does not explicitly involve electronic orbitals. There has been a renewed interest in orbital-free KE functionals recently, with many new functionals being developed.[23−31] Although orbital-free KE functionals are generally designed with free electron gas-like systems in mind,[24] it is appropriate that this approach also be thoroughly tested for modeling complex physical systems, involving chemical and structural changes on a large scale. In this paper, we test the applicability of orbital-free KE functionals to $NaAlH_4$ and some related systems, by considering a variety of KE functionals. Not only is $NaAlH_4$ an important material as a potential hydrogen storage medium, it may also be viewed as a challenging test system as it exhibits both ionic bonding [between Na^+ and $(AlH_4)^-$] and covalent bonding with significant ionic character [within the $(AlH_4)^-$ unit].[32,33]

2. Orbital-Free DFT

Within Hohenberg−Kohn density functional theory[21] the electronic energy is expressed in terms of functionals of the electron density $\rho(\mathbf{r})$

$$E_e[\rho] = T_s[\rho] + J[\rho] + V_{ie}[\rho] + E_{xc}[\rho] \qquad (1)$$

where $T_s[\rho]$, $J[\rho]$, $V_{ie}[\rho]$, and $E_{xc}[\rho]$ are the kinetic, Hartree, ion−electron Coulomb attraction (also called external potential), and exchange-correlation energy functionals.[22] The Kohn−Sham (KS-DFT)[34] and orbital-free (OF-DFT)[35,36] density functional

* To whom correspondence should be addressed. E-mail: T.Frankcombe@chem.leidenuniv.nl.

10.1021/jp050191y CCC: $30.25
Published on Web 08/10/2005

theories differ in the treatment of the KE term $T_s[\rho]$. The differences have a fundamental influence on the representation of $\rho(\mathbf{r})$ and the computational methods used to calculate the electronic energy.

The popular KS-DFT approach assumes a set of noninteracting particles, represented by the single-particle wave functions $\psi_i(\mathbf{r})$, which exactly reproduce the true electronic density ρ

$$\rho(\mathbf{r}) = \sum_i |\psi_i(\mathbf{r})|^2 \tag{2}$$

With this assumption, the KE is then given exactly by the expression implied by a Slater determinant

$$T_s[\rho] = \sum_i \left\langle \psi_i \left| -\frac{1}{2}\nabla^2 \right| \psi_i \right\rangle \tag{3}$$

Note that the difference between $T_s[\rho]$ and the true KE for interacting electrons is accounted for in $E_{xc}[\rho]$. The Kohn−Sham orbitals must be orthonormal (that is, $\langle\psi_i|\psi_j\rangle = \delta_{ij}$) to reflect their fermionic nature. The orthonormality conditions lead to the typical $O(N^3)$ scaling of KS-DFT calculations, though approximately linear scaling implementations can be constructed by employing further approximations such as localization of the orbitals.[37]

In contrast, OF-DFT uses an approximate form for the KE functional that does not rely on the orthogonality of some set of orbitals. The electron density is typically represented as the value of the density or its square root at a set of discrete points throughout space. Convergence with respect to the grid density is required, rather than the basis set and "k-space" sampling of traditional DFT. Performing part of the computation in reciprocal space using Fast Fourier Transforms allows all the required quantities to be obtained with computational effort that scales linearly or near-linearly with the size of the system.[35,36] Approaches that allow near-linear scaling in purely real space OF-DFT implementations are also being developed.[38,39]

There is presently no known orbital-free KE functional that exactly reproduces the Kohn−Sham KE of a general electron density ρ. Nonetheless, many approximate KE functionals exist in the literature which have been derived from different considerations (see, for example, Tran and Wesołowski[31] and references therein). The oldest KE functional is the so-called Thomas-Fermi expression[40,41]

$$T_{TF}[\rho] = C_{TF} \int \rho^{5/3}(\mathbf{r})\, d\mathbf{r} \tag{4}$$

with $C_{TF} = 3/10(3\pi^2)^{2/3}$, which is exact in the uniform electron gas limit. Another early functional is the von Weizsäcker energy[42]

$$T_{vW}[\rho] = \int \sqrt{\rho(\mathbf{r})}\left(-\frac{1}{2}\nabla^2\right)\sqrt{\rho(\mathbf{r})}\, d\mathbf{r} = \frac{1}{8}\int \frac{|\nabla\rho(\mathbf{r})|^2}{\rho(\mathbf{r})}\, d\mathbf{r} \tag{5}$$

which is exact for a single orbital. A useful functional is formed by combining the Thomas-Fermi and von Weizsäcker terms with an adjustable parameter λ:

$$T_{TF+\lambda W}[\rho] = T_{TF}[\rho] + \lambda T_{vW}[\rho] \tag{6}$$

Although rigorous derivation from the conventional gradient expansion gives $\lambda = 1/9$, numerical tests for atoms suggest $\lambda = 1/5$ gives results closer to those obtained with the Kohn−Sham KE expression.[22]

There exists an important group of KE functionals based on linear response theory. These functionals take the form

$$T_s[\rho] = T_{TF}[\rho] + T_{vW}[\rho] + T_K[\rho] \tag{7}$$

where the kernel term $T_K[\rho]$ is expressed as

$$T_K[\rho] = C_{TF}\int\int \rho^{\alpha}(\mathbf{r})\omega(\mathbf{r},\mathbf{r}')\rho^{\beta}(\mathbf{r}')\, d\mathbf{r}\, d\mathbf{r}' \tag{8}$$

Obviously different functionals of this class are determined by the constants α and β and the kernel function ω. A standard treatment based on the linear response of the noninteracting electron gas leads to a simple expression in reciprocal space for ω when it is taken to be density-independent.[30,35,36]

In this work, we use the Thomas-Fermi functional (TF), the combined TF+λW functional with $\lambda = 1/5$, and two linear response functionals to evaluate the accuracy of the OF-DFT approach. The latter functionals were developed by Wang, Govind, and Carter,[23,24] who showed first that the choice

$$\{\alpha,\beta\} = \frac{5}{6} \pm \frac{\sqrt{5}}{6} \tag{9}$$

was optimal for the density-independent kernel, and subsequently proposed a density-dependent kernel of the form $\omega(\mathbf{r},\mathbf{r}') = \omega(\xi_\gamma(\mathbf{r},\mathbf{r}'),\mathbf{r} - \mathbf{r}')$, where $\xi_\gamma(\mathbf{r},\mathbf{r}')$ is the two-body Fermi wave vector,[23,24,43] a geometric mean of the local one-body Fermi wave vectors $k_F(\mathbf{r})$ and $k_F(\mathbf{r}')$. These KE functionals will be denoted WGC-DI and WGC-DD for the density-independent and density-dependent kernel functionals, respectively.

2.1. Local Pseudopotentials. For computational efficiency, the nuclear-electron attractive Coulomb potential giving rise to the $V_{ie}[\rho]$ term in the total electronic energy is often replaced by a pseudopotential. The electronic density ρ then becomes a pseudodensity of valence electrons. Thus, the electron density being described is far less peaked around atomic nuclei and is easier to represent numerically.

The main advantage of using OF-DFT is the ability to construct linear-scaling implementations by avoiding orbital orthogonalization. The lack of orbitals within the OF-DFT framework introduces the limitation that only local pseudopotentials can be used to describe the external potential. That is, whereas most modern pseudopotentials (such as norm-conserving[44] or ultra-soft[45] pseudopotentials) can be described as nonlocal, containing several angular momentum contributions, the lack of orbitals in OF-DFT requires that the pseudopotential must be independent of angular momentum character, thus a function of the radius only.

3. Application to $NaAlH_4$

A simple test of the applicability of OF-DFT to the study of crystalline $NaAlH_4$ and its decomposition products is the calculation of the reaction energy for the reaction

$$NaAlH_4 \rightarrow NaH + Al + \frac{3}{2}H_2 \tag{10}$$

Obviously calculating the reaction energy for eq 10 requires the calculation of the total energy for each of the four phases involved, including full geometry optimization to the correct equilibrium structure for each phase. The geometry optimizations and total energy calculations performed in this work for the four phases in eq 10 will be outlined briefly in the following section for traditional KS-DFT and in more detail in sections

TABLE 1: Lattice Constant *a* for Al and NaH and Bond Length of the H_2 Molecule (Å)

	Al	NaH	H_2
TF	10.129	6.7003	1.53
TF+λW	4.2353	5.6047	1.50
WGC-DI	4.0332	5.5031	0.389
WGC-DD	4.0324	4.6500	−
KS-DFT LDA	3.9453	4.6180	0.767
KS-DFT PW91	4.0366	4.7054	0.754
experiment	4.0495[a]	4.890[b]	0.74[c]

[a] Reference 57. [b] Reference 58. [c] Reference 59.

3.2 to 3.4 for OF-DFT. Our OF-DFT calculations were performed using Hoffa, an OF-DFT code developed at Harvard. The Perdew−Zunger local density approximation (LDA) exchange-correlation functional[46] was used. The local pseudopotentials used were the evanescent core local pseudopotential of Fiolhais et al.[47] for sodium, the Goodwin, Needs, and Heine[48] local pseudopotential for aluminum, and a local Troullier-Martins-type pseudopotential[49] generated with the fhi98PP program of Fuchs and Scheffler[50] for hydrogen. Lattice constants were calculated by stress minimization.

3.1. KS-DFT Results. To serve as a benchmark for the subsequent OF-DFT calculations, we have performed calculations using traditional KS-DFT, with ultra-soft pseudopotentials[45] and the Dacapo package.[51,52] For these calculations the plane-wave cutoff energy and reciprocal space grid (using Monkhorst-Pack sampling[53]) were adjusted to give total energy convergence to within around 50 meV for each cell. Both the Perdew−Zunger LDA[46] and PW91 generalized gradient approximation[54] exchange-correlation functionals were used. The calculations with the PW91 exchange-correlation functional, in particular, gave very good agreement with experiment (Table 1) for the bulk lattice constants of Al (0.3% error), NaH (3% error), and $NaAlH_4$ (1% error) and the bond length of the H_2 molecule (1.7% error). The calculated reaction energy for the reaction in eq 10 was 44.0 kJ/mol H_2 using the PW91 exchange-correlation functional, which compares reasonably well with the experimentally measured[55] enthalpy at 25 °C of 37.7 kJ/mol H_2, and the more recent measurement[15] of 35 kJ/mol H_2. The reaction energy calculated within the LDA was 48.9 kJ/mol H_2.

3.2. OF-DFT: Al and NaH. The calculated lattice parameters that minimize the total energy for cubic close-packed Al and the rock salt structure NaH, using the various KE functionals in OF-DFT, are shown in Table 1. As expected,[24,28,38,56] the OF-DFT calculations for Al performed very well, requiring a density of grid points of around 10 $Å^{-1}$ in each dimension to achieve convergence of the total energy in the TF case, with the other three functionals requiring around half that density of grid points. The two functionals of Wang, Govind, and Carter (WGC-DI and WGC-DD) in particular gave lattice parameters of comparable accuracy to the KS-DFT PW91 calculations, around 0.4% smaller than the experimental value; this is around 2% larger than the KS-DFT LDA result, to which one would expect the OF-DFT calculations to be more similar because of the use of the LDA exchange correlation functional in both. The TF+λW KE functional also performed acceptably, giving a 5% overestimation of the lattice constant, whereas the TF functional performed poorly, overestimating the lattice constant by a factor of 2.5.

From the point of view of the lattice parameter, NaH was described quite well when using the WGC-DD functional. The resultant lattice parameter differed by 0.7% from the KS-DFT result when using the same LDA exchange-correlation functional. Unlike the Al case, the WGC-DI functional did not perform significantly better than the TF+λW functional, with both significantly overestimating the lattice parameters. The TF functional again performed poorly, although the result is not as bad as in the case of bulk Al.

3.3. OF-DFT: H_2 and the Failure of the Density-Dependent Kernel Evaluation. In periodic calculations, molecules are modeled using cells that are large enough to reduce interactions of nearest neighbors to negligible levels. However, many KE functionals are not expected to perform particularly well with cells containing large vacuum regions as the resultant large variations in the electron density cause a breakdown of the linear response approximations on which they are built.[24,36,60] Thus, in OF-DFT calculations, the cell in which the molecule is placed should be as small as can be attained to minimize the vacuum region. Of the two competing considerations, having a cell sufficiently large to remove intermolecular interaction artifacts is the more important. Therefore, an accurate OF-DFT KE functional must be able to handle the presence of vacuum regions and should be tested in this respect.

For H_2, we performed calculations on a H_2 molecule centered in a cubic cell and aligned with a cell edge. We found that for a H−H bond length of 0.75 Å, a cell of edge length 8−10 Å was sufficient to converge the total energy, similar to the analogous KS-DFT calculation using Dacapo.

When the H_2 bond length was relaxed using the TF and TF+λW functionals, the result was a large H−H distance of around 1.5 Å, as indicated in Table 1. The failure of the simple TF model is not surprising, since it has been shown that this model does not produce molecular binding.[22,61] The fact that the molecule did not dissociate totally in our calculation may be related to the presence of periodic boundary conditions. The WGC-DI functional also produced an incorrect structure for H_2, but with an excessively short bond. KS-DFT calculations with the local pseudopotentials used in the OF-DFT calculations produced a stable and accurate bond length of 0.745 Å, showing that the KE functional is responsible for the OF-DFT failures.

Calculations using the WGC-DD KE functional failed in a completely different way. The electronic energy did not converge to a reasonable value for any bond and cell edge length. The mode of failure was independent of the density relaxation method, of which three were applied: conjugate gradient, steepest descent, and a second-order equation of motion formulation.[24] The total energy varied apparently chaotically with the grid-point density used to represent ρ, from a factor of 2 to many orders of magnitude too large. The origin of this error can be readily traced to the way the KE is evaluated with this functional. The density dependence of the kernel function defining this particular functional means that for an efficient implementation the KE is evaluated by taking the Taylor expansion of the kernel function $\omega(\xi_\gamma(\mathbf{r},\mathbf{r}'),\mathbf{r}-\mathbf{r}')$ around some reference uniform density (that is, constant ξ_γ).[23,24,36,38] Wang, Govind, and Carter originally gave the reciprocal space expressions required for the evaluation of this Taylor expansion up to second order. This second-order expansion was used in the present work. For the electronic densities in solids for which the second-order expansion is successful, the first- and second-order contributions to the kernel term of this KE functional are many orders of magnitude smaller than the zeroth-order term. However for the case of the H_2 molecule in a box, minimizing the total energy along the direction given by $\partial E_e[\rho]/\partial\rho$, for example, starting from the initial guess uniform density, increased the first- and second-order contributions to $T_{\text{WGC-DD}}$ to values comparable to the zeroth-order term and as a consequence the total KE grew rapidly. This suggests that the

$O(\Delta\rho^3)$ and higher order terms in the Taylor expansion of $\omega(\xi_\gamma(\mathbf{r},\mathbf{r}'),\mathbf{r}-\mathbf{r}')$ are significant for this calculation, so that the second-order expansion is a poor approximation to the correct density dependence.

The various failures of the OF-DFT calculations for H_2 are not necessarily insurmountable obstacles to calculating reaction energies for hydrogen release and uptake reactions. Although no reasonable direct calculation of the energy of the reaction in eq 10 could be completed consistently using OF-DFT results for all phases, if the H_2 calculation were the only failure of the OF-DFT method then the total energy of H_2 could be treated as a single adjustable parameter, selected to, for example, reproduce the experimentally observed enthalpy of the reaction in eq 10. This quantity could then be transferred to situations such as the decomposition of $NaAlH_4$ to Na_3AlH_6 and further hydrogen release reactions.

3.4. OF-DFT: $NaAlH_4$. Total energy calculations for the $NaAlH_4$ crystal at the lattice constant and structure determined experimentally by Hauback et al.[62] were easily completed with the TF, TF+λW, and WGC-DI KE functionals. Again calculations using the WGC-DD KE functional failed with the electronic energy converging to a large negative value due to first- and second-order contributions to the kernel energy which were of comparable magnitude to the zeroth-order term.

Although evaluating the total energy using the other three KE functionals was routine, the application of these KE functionals led to a different mode of failure when attempting to optimize the $NaAlH_4$ structure. In all three cases, optimizing the positions using the forces calculated from the electronic density that minimized the total energy at each step[63] initially yielded similar behavior. The eight heavy aluminum and sodium ions moved only slightly away from their original positions, with displacements of the order of 0.01 Å. The hydrogen ions, on the other hand, underwent significant displacements. The calculated forces acted to dissociate the Al−H bonds and move the hydrogen ions to interstitial sites. This transition is indicated in Figure 1. In the case of the TF+λW KE functional, once the structure reached this point with dissociated $(AlH_4)^-$ units, the heavy-ion backbone also moved under the influence of large spurious forces and rapidly lost its well-ordered structure as the energy minimization proceeded.

As one would expect, the failure of the geometry optimizations was indicative of an incorrect description of the total energies, even at the experimental geometry. No attempt to obtain a reaction energy for the reaction in eq 10 from the OF-DFT results, whether using the calculated energy at the experimental structures or the results of the structural relaxations, produced a reasonable value.

3.5. OF-DFT: AlH_3. The tendency of the hydrogen ions to move to positions far from the aluminum ions suggests that the Al−H bond is not being well described by the OF-DFT KE functionals. To test this hypothesis, we performed calculations for the AlH_3 crystal, a structure in which each aluminum atom is octahedrally coordinated to six hydrogen atoms. Each hydrogen atom forms a bridge to another aluminum atom in what is likely to be a 3 center-2 electron bond.[64] Although this bonding seems significantly different from the bonding found in the $(AlH_4)^-$ units of $NaAlH_4$, modeling the structure of AlH_3 represents a reasonable test of the performance of OF-DFT in describing the Al−H interaction.

First, KS-DFT calculations were performed using both Dacapo and the ABINIT code[65] to optimize the AlH_3 crystal structure. Although the Dacapo calculations used the same ultrasoft pseudopotentials as those used in the calculations described above, the ABINIT calculations used the nonlocal pseudopotentials provided with that package (that is, Hamann-type[66] for aluminum and Goedecker−Teter−Hutter[67] for hydrogen, together denoted GTH−H). The PW91 and LDA exchange-correlation functionals were used for the Dacapo calculations while the calculations with ABINIT used only the LDA exchange-correlation functional. Both the Dacapo and ABINIT KS-DFT structural relaxation calculations resulted in structures very close to the experimentally determined structure.

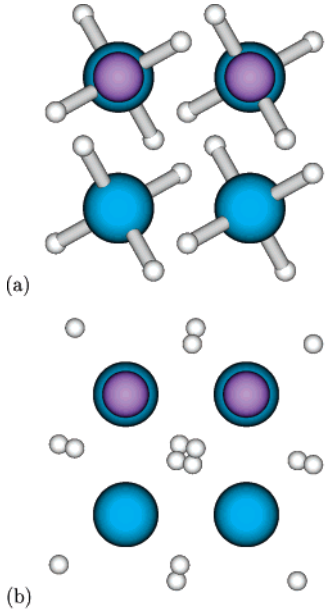

Figure 1. Structure of $NaAlH_4$, viewed along the *c* axis of a single unit cell. The larger, blue circles represent aluminum ions, with the smaller, purple sodium ions visible above them for the upper two, where the sodium ions are higher in the cell in the *c* direction. The smaller, white circles represent hydrogen ions. (a) The experimental structure of Hauback et al.[62] The $(AlH_4)^-$ tetrahedra are clearly visible. (b) The result of optimizing the ion positions using the WGC-DI KE functional. The hydrogen ions are scattered around the unit cell; the apparent clustering of the hydrogen ions in the center and at the edges of the diagram are a result of the orientation of the viewpoint along the *c* axis; these ions are separated by almost 3 Å.

In our OF-DFT implementation, the WGC-DD KE functional was again unstable. However, for low densities of grid points, using the second-order equation of motion optimization algorithm[24] for the electronic density made it possible to obtain the electronic energy for AlH_3 at the experimental structure. The range of densities of grid points for which the calculation was stable did not allow the convergence of the electronic energy to a reasonable level. The geometry optimization algorithm was unstable when the electron density was described by these low grid-point densities.

The use of the other three KE functionals was also problematic for the structure of AlH_3: the H-bridged structure found experimentally, as well as with KS-DFT calculations, could not be reproduced. For the TF and TF+λW KE functionals, the behavior was similar to that observed for $NaAlH_4$. The hydrogen ions were displaced away from the practically stationary aluminum ions to positions almost maximally distant from the aluminum ions. This structure is shown in Figure 2. For the WGC-DI KE functional, four of the six hydrogen ions around each aluminum ion behaved this way, maximizing the Al−H distance. The remaining two hydrogen ions moved close to the aluminum ion and formed a linear AlH_2 unit with a unrealistically short Al−H bond length of 1.15 Å.

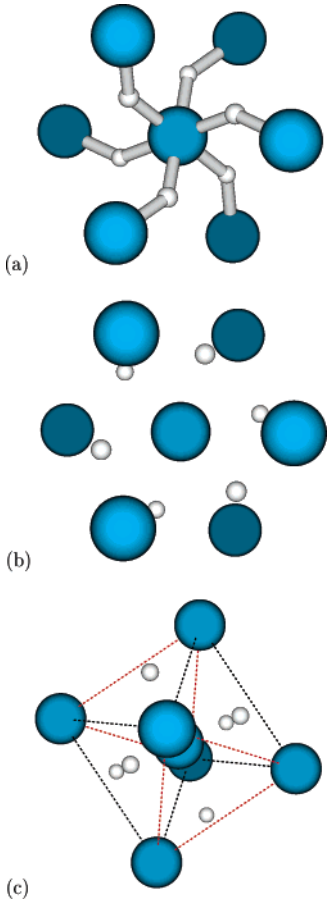

Figure 2. Structure of AlH_3. The larger, blue circles represent aluminum atoms, while the smaller, white circles represent hydrogen atoms. Only the hydrogen atoms coordinated to the central aluminum atom are shown, along with the aluminum atoms to which they form a bridge. Perspective has been added to emphasize the structure. (a) The experimental structure from Turley and Rinn,[64] viewed along the *c* axis of the hexagonal cell to emphasize the octahedral coordination within the structure. Two sets of three aluminum atoms form planes parallel to the page, with the central atom between those planes. (b) The result of optimizing the ionic positions within OF-DFT, using the TF+λW functional. The hydrogen ions have moved to six of the faces of the octahedron formed by the aluminum ions. (c) The structure shown in (b) with emphasis on the Al octahedron. The two faces of the octahedron without a hydrogen ion are shown in red and lie at the lower right front and upper left rear; the remaining edges are shown in black. The view shown in (b) is through the upper rear red-highlighted face of the octahedron shown in (c).

The results presented so far indicate that OF-DFT fails to reproduce a reasonable structure for systems involving Al−H bonds, whereas KS-DFT provides an accurate description of such systems. There are two elements which differ between these OF-DFT and KS-DFT calculations: the KE functional and the nature of the pseudopotentials employed. To determine which of the two was responsible for the failure of the OF-DFT approach, the calculations on AlH_3 were repeated within KS-DFT with the ABINIT package, using the same local pseudopotentials as the ones employed in the OF-DFT calculations. The optimized structure obtained from these calculations was essentially the same as the experimentally observed one. These results are shown in Table 2.

As can be readily seen from Table 2, the local pseudopotentials are not responsible for the poor description of the Al−H interaction observed with OF-DFT, since they give results of comparable quality to other pseudopotentials when employed within the KS-DFT approach. The failure of the calculations on AlH_3 (and thus likely on $NaAlH_4$) can be attributed exclusively to deficiencies of the KE functional employed within the OF-DFT approach.

TABLE 2: Structural Parameters of AlH_3: the Al−H Bond Length (Å) and the Bridging Al−H−Al Angle (degrees) as a Function of Formalism (KE), Pseudopotential (V_{psp}) and Exchange-Correlation Functional (E_{xc})

KE	V_{psp}	E_{xc}	Al−H bond length	bridge angle
KS-DFT	ultra-soft	PW91	1.714	141.3
KS-DFT	ultra-soft	LDA	1.712	141.8
KS-DFT	GTH−H	LDA	1.725	139.4
KS-DFT	local	LDA	1.720	140.3
TF+λW	local	LDA	2.105	100.5
experimental			1.715[a]	141.2[a]

[a] Reference 64.

4. Electron Density

The KE functional affects the calculation of Hellmann−Feynman forces on which structural optimization is based through the electron density that minimizes the electronic energy. Thus, the spurious forces that lead to the incorrect geometry for H_2, $NaAlH_4$ and AlH_3 must be attributed to the fact that the OF-DFT KE functionals give rise to an incorrect electron density. It is therefore instructive to examine the electron density that minimizes the electronic energy with the OF-DFT KE functional. In this section, the densities arising from OF-DFT calculations are compared with densities from KS-DFT calculations using the same local pseudopotentials and LDA exchange-correlation functional. The TF KE functional will not be considered here, being the least accurate of all of the KE functionals examined. To remove any dependence on the structure, we will rely on the experimental geometries of the five phases considered in this work as the basis for the comparison of electron densities.

The electron density calculated with KS-DFT for Al does not exhibit wide variations from the average density, as one would expect from a metal with well-behaved pseudopotentials. Three of the tested OF-DFT KE functionals give generally very good results for solid aluminum (Table 1). Correspondingly, the electron densities which minimize the electronic energy derived from the OF-DFT KE functionals agree well with that calculated within KS-DFT. All three of the successful OF-DFT KE functionals lead to electron densities varying from the KS-DFT values of the density by at most 2%.

Table 1 shows that all of the OF-DFT KE functionals tend to overestimate the NaH lattice constant, but the system is described reasonably. Close examination of the electron density along the Na−H direction shows that the OF-DFT KE functionals do not accurately reproduce the KS-DFT electron density, as shown in Figure 3. Generally speaking, both KS-DFT and OF-DFT result in electron density being drawn away from the metal ions toward the hydrogen ions. Clearly the OF-DFT KE functionals without a density-dependent kernel place too much of the electron density close to the hydrogen ions, while the density-dependent KE functional appears to over-correct this deficiency.

For the H_2 molecule, the TF+λW and WGC-DI KE functionals again concentrate the electron density excessively, but not in a simple manner as in the NaH case. The results are presented in Figure 4. The TF+λW KE functional draws too much electron density to the hydrogen ions at the expense of the bond region, weakening the bond and ultimately leading to the excessively long bond length reported in Table 1. The WGC-

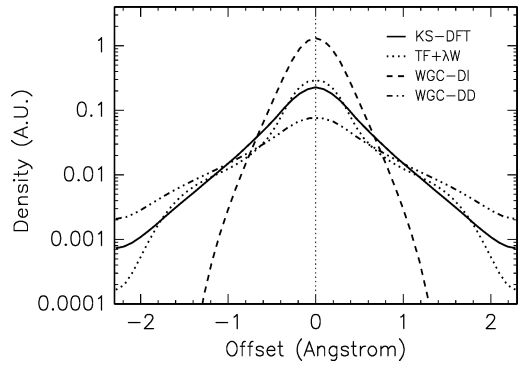

Figure 3. Electron density along one edge of the FCC cell of solid NaH. The edge passes from the position of one sodium ion at the right of the *x* axis to another at the left, through the position of a hydrogen ion at the center marked with a vertical line.

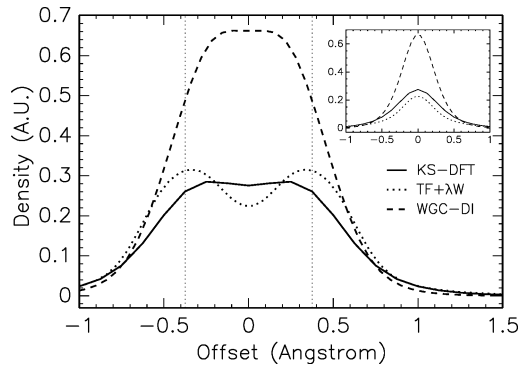

Figure 4. Electron density along the line of the bond in H_2. The vertical lines denote the positions of the hydrogen ions. The inset shows the density along a perpendicular bisector of the bond.

DI functional causes a large build-up of electron density in the bond region, yielding a very strong covalent character to the bond which presumably is the source of the force drawing the hydrogen ions closer together when the geometry is optimized. The inset in Figure 4 shows the density along a line perpendicular to and bisecting the line of the H_2 bond. Examining this density reveals that the increased electron density in the center of the bond obtained with the WGC-DI KE functional comes at the expense of electron density relatively far from the bond axis, in regions farther than 0.6 Å from the line of the bond.

Figure 5 shows contour plots of the electron density of AlH_3 in a plane containing one pair of the Al−H−Al bridges of the six surrounding a central aluminum ion. As in the NaH case, electron density is drawn away from the metal ions to the hydrogen ions. The covalent bonding character of the Al−H bonds is clearly visible as increased electron density along the Al−H bond regions compared to nonbond regions.

The TF+λW and in particular the WGC-DI KE functionals again cause an increased accumulation of electron density around the hydrogen ions, at the expense of the density around the aluminum ions and the bonding regions. Note that the density shown in Figure 5d for the WGC-DD KE functional was generated from one of the few low densities of grid points that yielded a convergent density. Despite this limitation, the density generated by the WGC-DD functional appears to follow the KS-DFT density the most closely out of the three OF-DFT densities shown.

The calculated electron density for $NaAlH_4$ is shown in Figure 6 for KS-DFT and for OF-DFT with the TF+λW and WGC-DI KE functionals. The plane chosen to display the density, indicated in Figure 6d, is slightly rotated along the *c* axis from a (210) plane. The plane contains one sodium ion and slices through one $(AlH_4)^-$ unit. As in the previous NaH and AlH_3

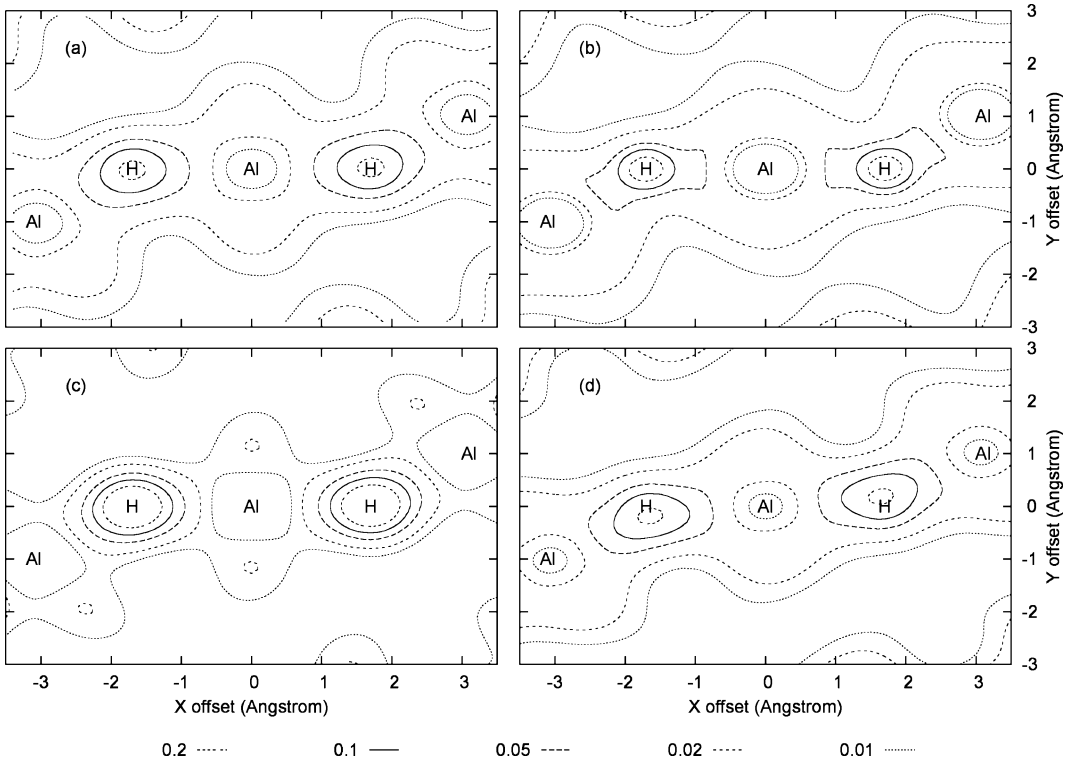

Figure 5. Contour plots of the electron density of AlH_3 on a plane containing Al−H−Al bridges. The density is expressed in atomic units. Aluminum ions are located in the regions of low density centrally and at either edge of the plot while two hydrogen ions form bridges in the regions of high density between the three aluminum ions. (a) The density calculated with KS-DFT. (b) The density calculated with OF-DFT using the TF+λW KE functional. (c) The density calculated with OF-DFT using the WGC-DI KE functional. (d) The density calculated with OF-DFT using the WGC-DD KE functional.

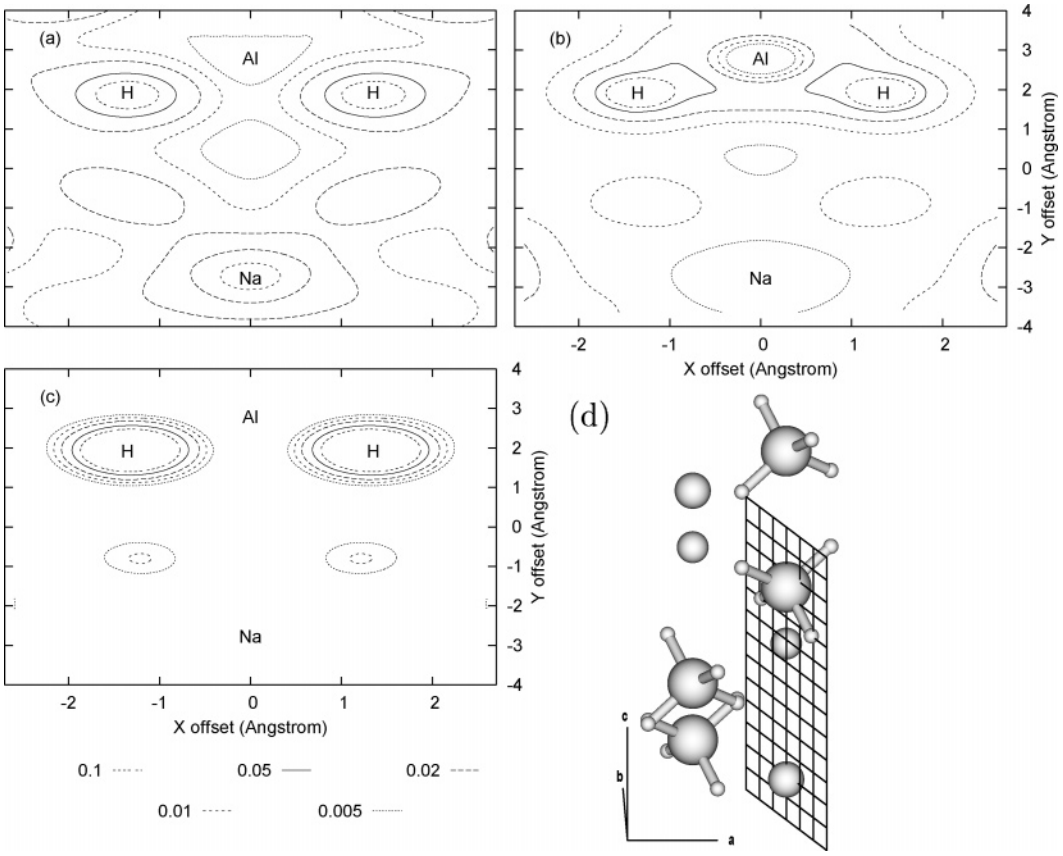

Figure 6. Contour plots of the density on a plane through the unit cell of $NaAlH_4$. The plane contains one aluminum, one sodium and two hydrogen ions, being similar to a (210) plane. The density is expressed in atomic units. (a) The density calculated with KS-DFT. (b) The density calculated with OF-DFT using the TF+λW KE functional. (c) The density calculated with OF-DFT using the WGC-DI KE functional. (d) The location of the plane for which the density is shown.

cases, electron density accumulates around the hydrogen ions at the expense of regions surrounding the metal ions.

Many of the differences between the KS-DFT and OF-DFT results shown in Figure 6 are similar to but more pronounced than those seen in the AlH_3 results of Figure 5. The TF+λW and WGC-DI KE functionals produce a much greater accumulation of electron density around the $(AlH_4)^-$ unit than arises from applying KS-DFT. Although the TF+λW functional places increased electron density in the $(AlH_4)^-$ region generally with no particular enhancement around the hydrogen ions, the WGC-DI KE functional leads to a dramatic increase in the electron density around the positions of the hydrogen ions, with nearly all the valence density occupying these regions.

5. Analysis of the Density-Dependent Kernel KE Functional Evaluation

A model electron density was used to further analyze the behavior of the WGC-DD KE functional. A three-dimensional Gaussian function was taken as the electron density distribution, normalized to describe the density of one electron. The density was centered in a cube of edge length 7.8 Å.

The KE given by the WGC-DD KE functional [eq 7] was evaluated as a function of the width parameter of the Gaussian function. The results are summarized in Figure 7, where the energy is decomposed into contributions from the T_{TF} and T_{vW} terms and each of the terms in the Taylor expansion for T_K. The total kinetic energy $T_{WGC\text{-}DD}$ (the sum of all of the displayed data) is not shown in Figure 7 but closely follows the second-order T_K term on the scale of the plot.

Clearly, the T_{TF}, T_{vW}, and zeroth-order T_K terms are well behaved as the width of the Gaussian function is decreased,

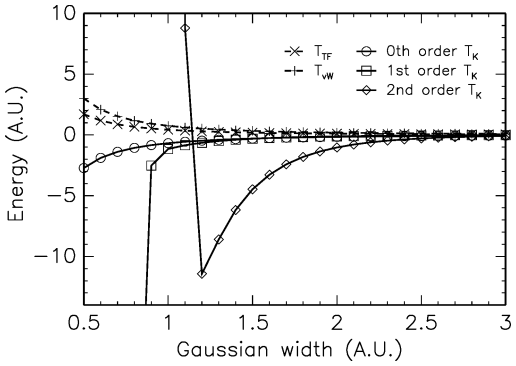

Figure 7. Contributions to $T_{WGC\text{-}DD}$ [eq 7] for a model electron density described by a Gaussian function.

which corresponds to a greater localization of the electron density and a greater variation in the density over space. On the other hand, the first- and second-order T_K terms tend to $-\infty$ and $+\infty$, respectively, as the Gaussian function width is decreased below 1 a.u.

Note that this testing with a fixed model density is very different to the testing reported by Zhou, Lignères, and Carter,[56] who monitored the energy terms contributing to $T_{WGC\text{-}DD}$ as the electronic density was relaxed for a test problem and found that neglecting the second-order term stabilized the KE functional evaluation.

Evaluation of the KE using the WGC-DI KE function was also performed for the model Gaussian function electron density. The density-independent kernel energies T_K are, on the scale of Figure 7, indistinguishable from the zeroth-order term in the

Taylor expansion of the density-dependent kernel energies for these Gaussian densities.

6. Conclusion

The computational effort of OF-DFT scales approximately linearly with system size. As such it is potentially a valuable tool for exploring complex chemical systems. Thus, OF-DFT must be tested for its applicability to complex chemical systems, given that the evaluation of the kinetic energy functional may lead to accuracy problems. To this end, we have tested the accuracy of OF-DFT applied to the hydrogen storage compound $NaAlH_4$, employing four well-known kinetic energy functionals. We have also considered the performance of OF-DFT for the related compounds NaH, Al, AlH_3, and H_2. The KE functionals tested were the Thomas-Fermi, mixed Thomas-Fermi-von Weizsäcker (using 1/5 of the von Weizsäcker energy) and the linear response functionals of Wang, Govind, and Carter with density-independent and density-dependent kernel functions.

Wang, Govind, and Carter have shown their choice of parameters to be optimal for a linear response KE functional with a density-independent kernel.[23,24] Thus, this functional should perform better than other linear response functionals of this form, of which there are several.[27−30] It should also perform better than the simpler TF and TF+λW KE functionals, an expectation that is borne out by the results presented above for bulk Al and NaH. Both the TF+λW and WGC-DI KE functionals appear to cause excessive attraction of electron density to regions surrounding negatively charged ions. The advantage of using a linear response KE functional with a density-dependent kernel, a recent trend in KE functionals for use within OF-DFT, is confirmed by our present results for Al and NaH. However, the instability of the evaluation of the total energy using the current second-order Taylor expansion is a serious problem when using this kernel.

The calculations evaluating the WGC-DD KE functional for a model electron density show that the Taylor expansion of the density dependence is unsatisfactory. Even if the Taylor expansion could be evaluated beyond second order (which it cannot[56]) such an expansion would likely be divergent, or at least numerically unstable, as the first-order term diverges in the $\gamma = 2.7$ case originally recommended by the functional designers[24] and explored in this work. It would be interesting to explore other expansions of the density dependence of the density-dependent kernel function. One possibility is an analytic function approximation in an approach similar to that which has been found to be useful for expanding the reciprocal space dependence of KE functional kernels.[38] Presumably also the WGC-DD KE functional could be evaluated in real space to yield a stable calculation, at the cost of transforming the entire method from a near-linear scaling method to one that scales at least quadratically with the size of the system being modeled. Such a calculation would, however, allow a more elementary appraisal of the density-dependent kernel KE functional.

None of the four KE functionals used in this work produced satisfactory results for H_2, $NaAlH_4$, or AlH_3, with the Al−H interaction being particularly poorly described. The fact that optimization of the lattice parameter of NaH yields a reasonable value complicates the picture and shows that the presence of hydrogen alone is not sufficient to render the KE functionals unusable. However, even in the NaH case the electron density that results when the OF-DFT KE functionals are used differs significantly from the KS-DFT result. Using the OF-DFT KE functionals tends to result in far greater accumulation of electron density around the location of hydrogen ions than when using KS-DFT. The WGC-DI KE functional is particularly problematic in this regard. The fact that the AlH_3 structure is accurately described by KS-DFT calculations using the same local pseudopotentials as in the OF-DFT calculations, clearly indicates that the failure is not caused by the local pseudopotentials but by the KE functionals.

OF-DFT has great potential for calculations on large-scale systems. Although the set of KE functionals used in this work was not exhaustive, it includes some of the most recent and successful functionals available in the literature. The limitations of these functionals demonstrated by these calculations indicate that further development is necessary in order to make the approach useful for applications beyond the simulation of simple metals. In particular, the presence of covalently bonded units places stringent demands on the KE functionals.

Acknowledgment. T.J.F. thanks the Physics Department of Harvard University for its hospitality during his visit. We gratefully acknowledge Prof. Emily Carter and co-workers for constructive comments on the manuscript and for providing a preprint of ref 56 prior to publication. This work was partially supported by a MURI-AFOSR grant (N.I.C. and E.K., Grant No. F49620-99-1-0272) and a CW/NWO program grant (T.J.F. and G.J.K.).

References and Notes

(1) Schlapbach, L.; Züttel, A. *Nature* **2001**, *414*, 353.
(2) Service, R. F. *Science* **2004**, *305*, 958.
(3) Züttel, A. *Naturwissenschaften* **2004**, *91*, 157.
(4) Züttel, A.; Wenger, P.; Sudan, P.; Mauron, P.; Orimo, S. I. *Mater. Sci. Eng. B* **2004**, *108*, 9.
(5) Zhou, Y. P.; Feng, K.; Sun, Y.; Zhou, L. *Progress Chem.* **2003**, *15*, 345.
(6) Hirscher, M.; Becher, M. *J. Nanosci. Nanotechnol.* **2003**, *3*, 3.
(7) Chen, D.; Chen, L.; Liu, S.; Ma, C. X.; Chen, D. M.; Wang, L. B. *J. Alloys Compd.* **2004**, *372*, 231.
(8) Ding, R. G.; Lu, G. Q.; Yan, Z. F.; Wilson, M. A. *J. Nanosci. Nanotechnol.* **2001**, *1*, 7.
(9) Singh, R. K.; Gupta, B. K.; Lototsky, M. V.; Srivastava, O. N. *J. Alloys Compd.* **2004**, *373*, 208.
(10) Sun, D. L.; Srinivasan, S. S.; Chen, G. R.; Jensen, C. M. *J. Alloys Compd.* **2004**, *373*, 265.
(11) Song, Y.; Guo, Z. X.; Yang, R. *Phys. Rev. B* **2004**, *69*, 094205.
(12) Kuriiwa, T.; Tamura, T.; Amemiya, T.; Fuda, T.; Kamegawa, A.; Takamura, H.; Okada, M. *J. Alloys Compd.* **1999**, *293*, 433.
(13) Shao, H. Y.; Wang, Y. T.; Xu, H. R.; Li, X. G. *Mater. Sci. Eng. B−Solid State Mater. Adv. Technol.* **2004**, *110*, 221.
(14) Bogdanović, B.; Schwickardi, M. *J. Alloys Compd.* **1997**, *253*, 1.
(15) Bogdanović, B.; Brand, R. A.; Marjanović, A.; Schwickardi, M.; Tolle, J. *J. Alloys Compd.* **2000**, *302*, 36.
(16) Bogdanović, B.; Felderhoff, M.; Kaskel, S.; Pommerin, A.; Schlichte, K.; Schuth, F. *Adv. Mater.* **2003**, *15*, 1012.
(17) Kiyobayashi, T.; Srinivasan, S. S.; Sun, D. L.; Jensen, C. M. *J. Phys. Chem. A* **2003**, *107*, 7671.
(18) Arroyo y de Dompablo, M. E.; Ceder, G. *J. Alloys Compd.* **2004**, *364*, 6.
(19) Genma, R.; Okada, N.; Nishi, Y.; Uchida, H. H. *J. Japan Inst. Met.* **2003**, *67*, 440.
(20) Gross, K. J.; Guthrie, S.; Takara, S.; Thomas, G. *J. Alloys Compd.* **2000**, *297*, 270.
(21) Hohenberg, P.; Kohn, W. *Phys. Rev. B* **1964**, *136*, 864.
(22) Parr, R. G.; Yang, W. *Density-Functional Theory of Atoms and Molecules*; Oxford University Press: New York, 1989.
(23) Wang, Y. A.; Govind, N.; Carter, E. A. *Phys. Rev. B* **2001**, *64*, 089903(E).
(24) Wang, Y. A.; Govind, N.; Carter, E. A. *Phys. Rev. B* **1999**, *60*, 16350.
(25) Wang, Y. A.; Govind, N.; Carter, E. A. *Phys. Rev. B* **2001**, *64*, 129901.
(26) Wang, Y. A.; Govind, N.; Carter, E. A. *Phys. Rev. B* **1998**, *58*, 13465.
(27) Perrot, F. *J. Phys.: Cond. Matter* **1994**, *6*, 431.
(28) Smargiassi, E.; Madden, P. A. *Phys. Rev. B* **1994**, *49*, 5220.
(29) Wang, L.-W.; Teter, M. P. *Phys. Rev. B* **1992**, *45*, 13196.

(30) Pearson, M.; Smargiassi, E.; Madden, P. A. *J. Phys.: Cond. Matter* **1993**, *5*, 3321.
(31) Tran, F.; Wesłowski, T. A. *Int. J. Quantum Chem.* **2002**, *89*, 441.
(32) Peles, A.; Alford, J. A.; Ma, Z.; Yang, L.; Chou, M. Y. *Phys. Rev. B* **2004**, *70*, 165105.
(33) Aguayo, A.; Singh, D. J. *Phys. Rev. B* **2004**, *69*, 155103.
(34) Kohn, W.; Sham, L. J. *Phys. Rev.* **1965**, *140*, 1133.
(35) Wang, Y. A.; Carter, E. A. Theoretical Methods in Condensed Phase Chemistry; Schwartz, S. D., Ed.; In *Progress in Theoretical Chemistry and Physics*; Kluwer: Norwell, MA, 2000; p 117.
(36) Watson, S. C.; Carter, E. A. *Comput. Phys. Commun.* **2000**, *128*, 67.
(37) Goedecker, S. *Rev. Mod. Phys.* **1999**, *71*, 1085.
(38) Choly, N.; Kaxiras, E. *Solid State Commun.* **2002**, *121*, 281.
(39) Modine, N. A.; Zumbach, G.; Kaxiras, E. *Phys. Rev. B* **1997**, *55*, 10289.
(40) Thomas, L. H. *Proc. Cam. Philos. Soc.* **1926**, *23*, 542.
(41) Fermi, E. *Z. Phys.* **1928**, *48*, 73.
(42) von Weizsäcker, C. F. *Z. Phys.* **1935**, *96*, 431.
(43) Wang, Y. A. *Phys. Rev. A* **1997**, *55*, 4589.
(44) Hamann, D. R.; Schlüter, M.; Chiang, C. *Phys. Rev. Lett.* **1979**, *43*, 1494.
(45) Vanderbilt, D. *Phys. Rev. B* **1990**, *41*, 7892.
(46) Perdew, J. P.; Zunger, A. *Phys. Rev. B* **1981**, *23*, 5048.
(47) Fiolhais, C.; Perdew, J. P.; Armster, S. Q.; MacLaren, J. M.; Brajczewska, M. *Phys. Rev. B* **1996**, *53*, 13193.
(48) Goodwin, L.; Needs, R. J.; Heine, V. *J. Phys.: Cond. Matter* **1990**, *2*, 351.
(49) Troullier, N.; Martins, J. L. *Phys. Rev. B* **1991**, *43*, 1993.
(50) Fuchs, M.; Scheffler, M. *Comput. Phys. Commun.* **1999**, *119*, 67.
(51) Hammer, B.; Hansen, L. B.; Nørskov, J. K. *Phys. Rev. B* **1999**, *59*, 7413.
(52) Bahn, S. R.; Jacobsen, K. W. *Comput. Sci. Eng.* **2002**, *4*, 56.
(53) Monkhorst, H. J.; Pack, J. D. *Phys. Rev. B* **1976**, *13*, 5188.
(54) Perdew, J. P.; Chevary, J. A.; Vosko, S. H.; Jackson, K. A.; Pederson, M. R.; Singh, D. J.; Fiolhais, C. *Phys. Rev. B* **1992**, *46*, 6671.
(55) Smith, M. B.; Bass, G. E., Jr. *J. Chem. Eng. Data* **1963**, *8*, 342.
(56) Zhou, B.; Lignères, V. L.; Carter, E. A. *J. Chem. Phys.* **2005**, *122*, 044103.
(57) Donohue, J. *The structures of the elements*; John Wiley & Sons: New York, 1974.
(58) Williams, M. G.; Brown, S. R.; Cottrell, S. P. *Hyperfine Interact.* **1997**, *106*, 105.
(59) Lide, D. R., Ed. *CRC Handbook of Chemistry and Physics*; CRC Press: Boca Raton, FL, 2001; Vol. 82.
(60) Foley, M.; Madden, P. A. *Phys. Rev. B* **1996**, *53*, 10589.
(61) Teller, E. *Rev. Mod. Phys.* **1962**, *34*, 627.
(62) Hauback, B. C.; Brinks, H. W.; Jensen, C. M.; Murphy, K.; Maeland, A. J. *J. Alloys Compd.* **2003**, *358*, 142.
(63) Choly, N.; Kaxiras, E. *Phys. Rev. B* **2003**, *67*, 155101.
(64) Turley, J. W.; Rinn, H. W. *Inorg. Chem.* **1969**, *8*, 18.
(65) Gonze, X.; Beuken, J.-M.; Caracas, R.; Detraux, F.; Fuchs, M.; Rignanese, G.-M.; Sindic, L.; Verstraete, M.; Zerah, G.; Jollet, F.; Torrent, M.; Roy, A.; Mikami, M.; Ghosez, P.; Raty, J.-Y.; Allan, D. *Comput. Mol. Sci.* **2002**, *25*, 478.
(66) Hamann, D. R. *Phys. Rev. B* **1989**, *40*, 2980.
(67) Goedecker, S.; Teter, M.; Hutter, J. *Phys. Rev. B* **1996**, *56*, 1703.